



# Phase transformations and volume changes in spinel $\text{Li}_x\text{Mn}_2\text{O}_4$

A. Van der Ven, C. Marianetti, D. Morgan, G. Ceder\*

*Department of Materials Science and Engineering, Massachusetts Institute of Technology, 77 Massachusetts Avenue, Cambridge, MA 02139, USA*

## Abstract

First-principles methods have been used to calculate the phase diagram and volume expansion of spinel  $\text{Li}_x\text{Mn}_2\text{O}_4$  as a function of lithium content. The calculations confirm the experimentally observed two phase region between  $x = 1$  and 2 and the ordered phase at  $x = 1/2$ . In addition, the expected large step in voltage at  $x = 1$  is obtained. It is shown that these phenomena are qualitatively determined by the interactions of Li with each other and the  $\text{Mn}_2\text{O}_4$  host and only quantitatively influenced by the more subtle electronic effects such as Jahn–Teller distortions, charge ordering and magnetic excitations. The two-phase region between  $x = 1$  and 2 is found to be driven by strong repulsive interactions between lithium ions occupying adjacent tetrahedral 8a and octahedral 16c sites. The origin of the large volume change upon transforming from  $\text{LiMn}_2\text{O}_4$  to  $\text{Li}_2\text{Mn}_2\text{O}_4$  is also investigated from first principles. The possible sources of the volume change are identified to be the intercalated lithium, the Jahn–Teller distortion, and the introduction of anti-bonding  $e_g$  electrons into the Mn d-orbitals. The latter effect is found to be dominant. Some speculation is offered on how the large volume change upon lithiation of manganese dioxide can be prevented. © 2000 Elsevier Science B.V. All rights reserved.

**Keywords:**  $\text{Li}_x\text{Mn}_2\text{O}_4$ ; Spinel; Phase diagram; First principles; Jahn–Teller distortion; Anti-bonding  $e_g$  levels; Lithium intercalation; Battery material

## 1. Introduction

Spinel  $\text{Li}_x\text{Mn}_2\text{O}_4$  is a promising cathode material for rechargeable lithium batteries and exhibits a rich variety of electronic and electrochemical properties. In an electrochemical cell, the lithium concentration in  $\text{Li}_x\text{Mn}_2\text{O}_4$  can be varied over a large interval, causing the compound to undergo a series of phase transformations.  $\text{Li}_x\text{Mn}_2\text{O}_4$  differs from many other transition metal oxide intercalation compounds in that a range of electronic phenomena play a significant role in determining its thermodynamic and

structural properties: Jahn–Teller distortions [1–4], charge ordering [5,6] and magnetic ordering [7] have each been identified as producing measurable imprints on electrochemical characteristics. The presence of numerous electronic phenomena can cloak the true microscopic origins of different phase transformations and volumetric changes that occur during cycling of  $\text{Li}_x\text{Mn}_2\text{O}_4$ .

Spinel lithium manganese oxide is generally synthesized at the  $\text{LiMn}_2\text{O}_4$  composition, which is isomorphic with mineral  $\text{MgAl}_2\text{O}_4$  spinel and belongs to the  $Fd3m$  space group [8]. Within the  $\text{Mn}_2\text{O}_4$  host structure, lithium can reside in both the tetrahedral 8a and octahedral 16c sites. Lithium extraction from  $\text{LiMn}_2\text{O}_4$  occurs around 4.0 V and

\*Corresponding author. Fax: +1-617-258-6534.

E-mail address: gceder@mit.edu (G. Ceder).

proceeds in two stages separated by a step of approximately 0.1 V [3]. The step has been attributed to Li ordering over half the tetrahedral sites at  $x = 1/2$  [9]. Below  $x = 1/2$ , a two phase region is observed between two cubic forms of  $\text{Li}_x\text{Mn}_2\text{O}_4$  with  $x = 0.15$  and  $x = 0.4$  [3,10]. Between  $x = 1/2$  and 1, solid solution like behavior is often reported [3,10]. However, recent work on lithium excess  $\text{Li}_{x+y}\text{Mn}_{2-y}\text{O}_4$  has indicated the presence of a two phase region in this concentration range [11]. For  $x < 1$ , the lithium ions occupy the tetrahedral sites [3,8]. Lithium insertion into  $\text{LiMn}_2\text{O}_4$  proceeds at constant voltage around 2.9 V [1,3,12]. The 2.9 V plateau signifies a two phase region between cubic spinel  $\text{LiMn}_2\text{O}_4$  and  $\text{Li}_2\text{Mn}_2\text{O}_4$  having tetragonal symmetry as a result of a coordinated Jahn–Teller distortion of the cubic host [1,3]. In cubic  $\text{LiMn}_2\text{O}_4$  the lithium ions occupy the tetrahedral sites while in tetragonal  $\text{Li}_2\text{Mn}_2\text{O}_4$ , lithium predominantly occupies the octahedral sites [1,8]. This first order transition results in a large and anisotropic volume change which in turn causes severe damage to the cathode material during cycling.

Below room temperature, additional features have been observed. Cubic spinel  $\text{LiMn}_2\text{O}_4$  transforms to a distorted phase below  $T=280$  K according to a first order transition [4,13]. Initially this phase was identified as having tetragonal symmetry, though subsequent studies have shown it to have orthorhombic symmetry [14,15]. Recent neutron diffraction data has indicated the possibility of charge ordering in this phase [5,6]. Low temperature (below room temperature) investigations of the voltage profile of  $\text{Li}_x\text{Mn}_2\text{O}_4$  have exposed an additional step of 0.01 V around  $x=0.7$  flanked by small plateaus [16].

Phase transformations are generally detrimental for the cathode material as they are often accompanied by abrupt volume changes. In this paper, we investigate the microscopic origins of important phase transformations in  $\text{Li}_x\text{Mn}_2\text{O}_4$  from first principles. Combining a first-principles lattice model with Monte Carlo simulations, we demonstrate that the first order phase transformation between  $x=1$  and 2 is driven by strong repulsive interactions between lithium ions in adjacent tetrahedral and octahedral sites. Furthermore, first-principles electronic structure calculations indicate that the dominant contribu-

tion to the large volume change associated with this first order transition is the increase in the number of valence electrons in the antibonding  $e_g$  band, this effect being more important than the cooperative Jahn–Teller distortion. We show that transfer of the  $e_g$  electron into the minority spin  $t_{2g}$  band would lead to a manganese oxide intercalation host that undergoes a negligible volume change when lithiated. The lattice model also predicts that the lithium ions order at  $x=1/2$  into alternating tetrahedral sites as has often been speculated.

The paper is structured as follows. In Section 2, we describe the methodology of our first-principles investigation of  $\text{Li}_x\text{Mn}_2\text{O}_4$ . In Section 3, we present a first-principles phase diagram of cubic  $\text{Li}_x\text{Mn}_2\text{O}_4$  and we demonstrate that many of the electrochemical properties of  $\text{Li}_x\text{Mn}_2\text{O}_4$  occur even in the absence of Jahn–Teller distortions. The effect of Jahn–Teller distortions on the phase diagram and voltage curves is discussed in Section 4. In Section 5, we discuss the origin of the volume expansion occurring during the first order transition at 2.9 V.

## 2. Methodology

The basic approach of our investigation can be divided into two steps. In the first step, we performed first principles total energy calculations of spinel  $\text{Li}_x\text{Mn}_2\text{O}_4$  at different lithium concentrations. We used density functional theory [17] either within the local density approximation (LDA) [18] or within the generalized gradient approximation (GGA). These methods are approximations to the solutions of the many body Schrodinger equation of the solid. The accuracy of LDA and GGA in predicting properties of  $\text{Li}_x\text{Mn}_2\text{O}_4$  has been studied in Ref. [19]. From these calculations, detailed structural and electronic information about the compound as well as total energies that enable a comparison of relative stabilities can be obtained. To perform these calculations we have used the VASP plane wave pseudo-potential code [20,21]. All total energies were optimized with respect to volume and internal atomic positions and were spin polarized (ferromagnetic) unless explicitly mentioned.

In the second step, we used a subset of the calculated total energies corresponding to different

lithium vacancy arrangements within the  $\text{Mn}_2\text{O}_4$  cubic host structure to parameterize a lattice model [22,23]. The resultant lattice model describes how the lithium ions interact with each other and with the host structure. The usefulness of lattice models for the study of intercalation compounds has been discussed by McKinnon [24]. More recently, first-principles lattice models have been implemented to investigate both the layered and spinel forms of  $\text{Li}_x\text{CoO}_2$  [25–28]. The approach is based on the cluster expansion formalism [29] which allows for a natural way of describing the configurational energy in a multi-component crystal. Within this formalism, occupation variables  $\sigma_i$  are assigned to each lithium site  $i$  which are +1 (–1) if a lithium ion (vacancy) resides at site  $i$ . The configurational energy can be expanded in terms of polynomials  $\phi_\alpha$  according to

$$E = V_0 + \sum_{\alpha} V_{\alpha} \cdot \phi_{\alpha} \quad (1)$$

where

$$\phi_{\alpha} = \prod_{i \in \alpha} \sigma_i \quad (2)$$

are products of occupation variables associated with lithium sites belonging to clusters  $\alpha$ . These clusters are for example pairs, triplets, etc. of lithium sites. The coefficients  $V_0$  and  $V_{\alpha}$  are referred to as effective cluster interactions (ECI) and are determined by fitting to first-principles total energies [23,30]. Although formally the expansion extends over all possible clusters  $\alpha$  of Li sites, in practice it is truncated.

For  $\text{Li}_x\text{Mn}_2\text{O}_4$ , we constructed a lattice model describing the energetics of lithium and vacancy distribution over the combined set of tetrahedral 8a and octahedral 16c sites of the cubic  $\text{Mn}_2\text{O}_4$  spinel host. The tetrahedral 8a sites form a diamond network while the octahedral 16c sites reside between nearest-neighbor 8a sites. There are twice as many octahedral sites as tetrahedral sites. The ECI of the lattice model were determined by fitting to the energies (ferromagnetic spin-polarized LDA) of 21 different lithium vacancy arrangements in cubic  $\text{Mn}_2\text{O}_4$  using a linear programming technique [30]. Fig. 1 illustrates the clusters used in the cluster expansion and Table 1 lists the numerical values of the ECI.

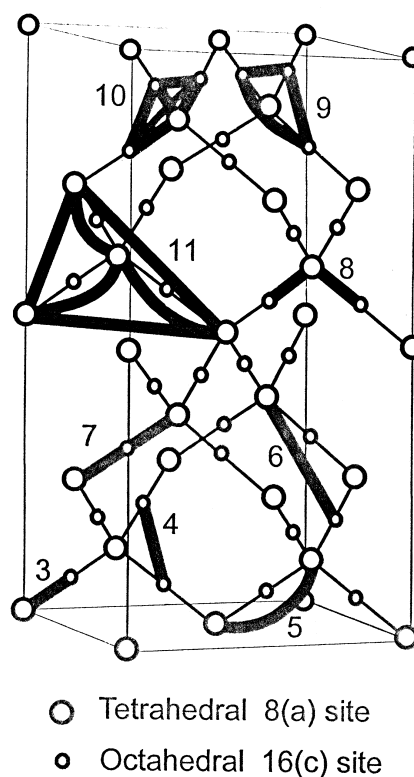


Fig. 1. Illustration of the clusters (connected by dark lines) used in the cluster expansion (i.e. the energy expression for the lattice model). Shown are the tetrahedral 8a and octahedral 16c sites. The positions of the Mn and O ions are not shown. The numbering next to each cluster refers to the ECI in Table 1.

### 3. Phase diagram and related properties of cubic $\text{Li}_x\text{Mn}_2\text{O}_4$

In this section, we investigate the topology of the phase diagram of cubic  $\text{Li}_x\text{Mn}_2\text{O}_4$ . An approximate phase diagram was determined by implementing the lattice model of Table 1 in canonical and grand canonical Monte Carlo simulations. Note that the lattice model only describes the energetics of different lithium vacancy arrangements within the *cubic* form of spinel  $\text{Mn}_2\text{O}_4$ . It does not account for Jahn–Teller distortions, any possible charge ordering, or the temperature dependence of magnetic ordering. In effect the lattice model of Fig. 1 and Table 1 enables us to investigate the properties of  $\text{Li}_x\text{Mn}_2\text{O}_4$  that arise solely from the interactions between the lithium ions with each other and with

Table 1  
Values of the ECI corresponding to the clusters in Fig. 1

Corresponding number in Fig. 1	Cluster descriptions	ECI (meV)
0	Empty cluster	87.4
1	Tetrahedral point cluster	171.4
2	Octahedral point cluster	154.0
3	Nearest-neighbor tetrahedral–octahedral pair	72.0
4	Nearest-neighbor octahedral–octahedral pair	22.6
5	Nearest-neighbor tetrahedral–tetrahedral pair	20.2
6	Second nearest-neighbor tetrahedral–octahedral pair	2.6
7	Tetrahedral–octahedral–tetrahedral triplet	11.9
8	Octahedral–tetrahedral–octahedral triplet	8.7
9	Octahedral triplet	4.5
10	Tetrahedral–octahedral quadruplet	7.6
11	Tetrahedral quadruplet	1.0

the host. Any qualitative discrepancy with experiment will then expose the role that more complex electronic phenomena play on the electrochemical properties of  $\text{Li}_x\text{Mn}_2\text{O}_4$ . In the next section, we will indicate how the inclusion of Jahn–Teller distortions alters the phase diagram and voltage curves.

The calculated phase diagram is illustrated in Fig. 2. The phase diagram is characterized by a large miscibility gap between  $x=1$  and 2 and by an ordered phase at  $x=1/2$ . The miscibility gap disappears above approximately 450 K. The ordered

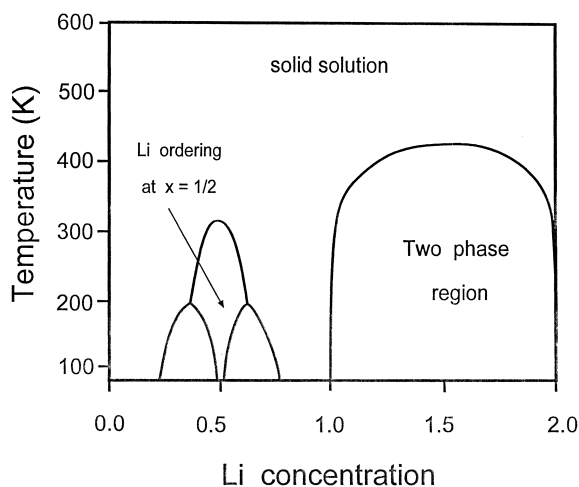


Fig. 2. Calculated phase diagram of  $\text{Li}_x\text{Mn}_2\text{O}_4$  using the lattice model of Fig. 1 and Table 1. This diagram was calculated neglecting contributions from Jahn–Teller distortions, charge ordering and the temperature dependence of magnetic ordering.

phase at  $x=1/2$  is stable until approximately 310 K. In the ordered phase, the lithium ions segregate to alternating tetrahedral sites; the ordering of lithium ions and vacancies on the tetrahedral sites is the same as that of Zn and S in zinc blende  $\text{ZnS}$ .

The simple phase diagram of Fig. 2 already captures some essential features observed in  $\text{Li}_x\text{Mn}_2\text{O}_4$ . Inaccuracies in predicted order–disorder transition temperatures are not uncommon in first-principles phase diagram calculations, however. In view of the neglect of Jahn–Teller distortions and related localized electronic phenomena, the calculated phase diagram can only be considered as an approximate qualitative representation of the true phase diagram. For example, a very obvious discrepancy with experiment is the absence at room temperature of a two phase region in the concentration range  $x=0$  and  $x=1/2$ . Although a two phase region between ordered  $\text{Li}_{1/2}\text{Mn}_2\text{O}_4$  and  $\text{Li}_x\text{Mn}_2\text{O}_4$  with  $x \sim 0.25$  is predicted in this concentration range, it disappears through a tricritical point around 200 K above which the order–disorder transition becomes second order. This is also predicted between  $x=1/2$  and 0.75. The existence of the tricritical points is likely an artefact of the particular lattice model used and may be absent in the actual phase diagram of  $\text{Li}_x\text{Mn}_2\text{O}_4$ . Likewise, the predicted order–disorder transition temperature of  $\text{Li}_{1/2}\text{Mn}_2\text{O}_4$  as well as the critical temperature of the miscibility gap should only be viewed as rough approximations of the actual temperatures.

Recent low-temperature electrochemical measurements of  $\text{Li}_x\text{Mn}_2\text{O}_4$  have shown that a new step in the voltage profile appears below approximately 275 K around  $x=0.7$  [16]. This step could be the result of lithium ordering. The LDA total energy calculations of the ordered lithium vacancy configurations considered predict additional ground states at  $x=0.25$  and  $x=0.75$ . These structures lie on the convex hull of the zero temperature formation energies, though they are almost degenerate in energy with a phase separation of the ground states at  $x=0$  and  $1/2$  and  $x=1/2$  and  $1$  respectively. The lattice model of Fig. 1 and Table 1 is a relatively short ranged one and is not able predict the structures at  $x=0.25$  and  $0.75$  as being ground states. Instead these structures are predicted by the lattice model to be exactly degenerate in energy with a phase separation of the ground states at  $x=0$  and  $1/2$  and  $x=1/2$  and  $1$  respectively. To remove this degeneracy, it would be necessary to include pair clusters and/or multibody clusters that extend over larger distances than are currently considered [22]. Nevertheless, we expect the ordering at  $x=1/2$  to be the dominant ground state between  $x=0$  and  $1$  and anticipate that the other ordered phases are only stable at low temperature.

Fig. 3a shows the tetrahedral and octahedral site occupancies as a function of overall lithium concentration at 275 K. Below  $x=1$ , the lithium ions predominantly occupy the tetrahedral sites and at  $x=1$  all the tetrahedral sites are occupied. As the lithium concentration is increased further, the miscibility gap is entered whereby  $\text{LiMn}_2\text{O}_4$  coexists with  $\text{Li}_x\text{Mn}_2\text{O}_4$  with  $x$  slightly less than 2. In the latter phase, lithium predominantly occupies the octahedral sites, though when  $x$  is slightly less than 2, lithium also occupies a small fraction of tetrahedral sites which are adjacent to empty octahedral sites. As the temperature increases, the same qualitative features continue to hold, however, thermal excitations result in a more significant occupation by lithium of octahedral (tetrahedral) sites at  $x=1$  ( $x=2$ ). For temperatures above the miscibility gap, there is a gradual displacement of lithium from the tetrahedral sites to the octahedral sites as the lithium concentration increases beyond  $x=1$ . This is illustrated in Fig. 3b.

A deeper understanding of the evolution of the

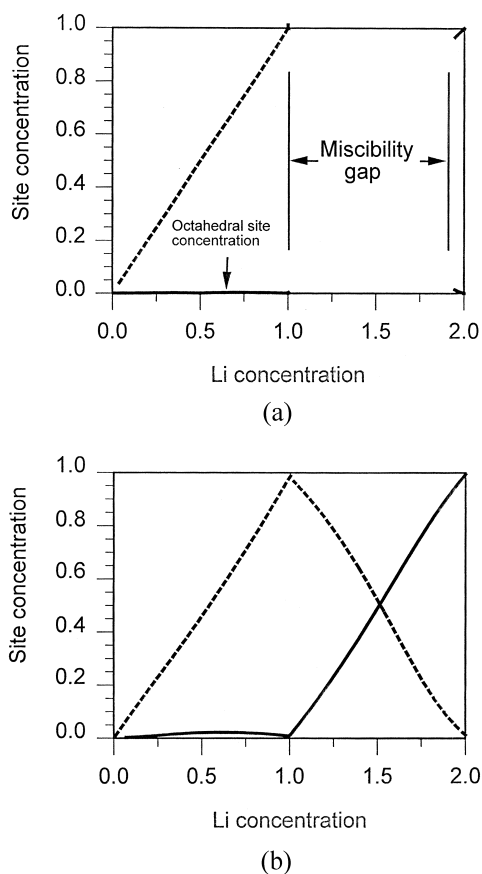


Fig. 3. Calculated tetrahedral (dashed lines) and octahedral (full lines) site concentrations as a function of overall lithium concentration (a) at 275 K and (b) at 500 K.

tetrahedral 8a and octahedral 16c site occupancies with lithium concentration can be obtained by inspection of the relative stability between the two sites. According to the cluster expansion of Table 1, an isolated lithium ion in an empty  $\text{Mn}_2\text{O}_4$  spinel host is more stable in a tetrahedral site than in an octahedral site by 160 meV. This explains the tetrahedral site occupancy below  $x=1$ . At  $x=1$ , the tetrahedral sites are saturated and further lithium addition must be accommodated by the energetically less favorable octahedral sites. The oxygen tetrahedra surrounding the 8a sites, however, share faces with the oxygen octahedra around the 16c sites. The proximity of these sites causes their simultaneous occupation by lithium to be energetically unfavorable as a result of electrostatic repulsion. This is reflected

by the large and repulsive nearest-neighbor tetrahedral–octahedral ECI of the cluster expansion of Table 1. As the octahedral site occupancy increases when  $x$  is raised above 1, the large electrostatic repulsion causes a displacement of lithium ions from tetrahedral sites to octahedral sites. Above the miscibility gap, this displacement occurs gradually. However as can be seen from Fig. 4, the fraction of occupied adjacent tetrahedral–octahedral site pairs is much lower than would be expected for a system with a random distribution of lithium over the tetrahedral and octahedral sites. As the temperature is lowered, thermal excitations no longer overcome the large electrostatic repulsion between lithium ions in these adjacent sites and a miscibility gap appears. The miscibility gap, therefore, arises from a competition between filling as many energetically favorable tetrahedral sites while at the same time minimizing the number of occupied nearest-neighbor tetrahedral–octahedral pairs.

For applications in a battery, the crucial thermodynamic property of  $\text{Li}_x\text{Mn}_2\text{O}_4$  is the voltage curve as a function of lithium concentration. The voltage is linearly related to the chemical potential of lithium within the cathode according to

$$V(x) = -\frac{(\mu_{\text{Li}}^{\text{cathode}} - \mu_{\text{Li}}^{\text{anode}})}{zF} \quad (3)$$

where  $z$  is the charge (in electrons) transported by Li in the electrolyte (i.e.  $z=1$  for Li),  $F$  is Faraday's

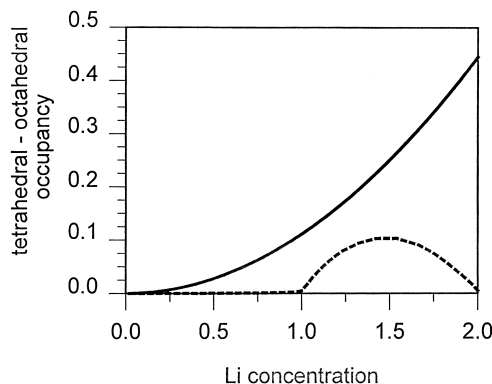


Fig. 4. Fraction of adjacent tetrahedral sites and octahedral sites that are simultaneously occupied by lithium at 500 K (dashed line) compared to the fraction for a random distribution of lithium over tetrahedral and octahedral sites (full line).

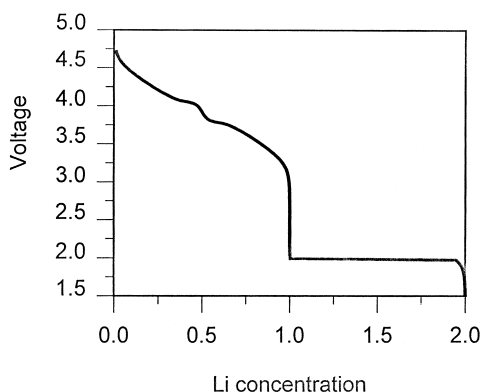


Fig. 5. Calculated voltage curve for  $\text{Li}_x\text{Mn}_2\text{O}_4$  as a function of Li concentration at 275 K.

constant,  $\mu_{\text{Li}}^{\text{cathode}}$  is the chemical potential of Li in the cathode and  $\mu_{\text{Li}}^{\text{anode}}$  is the chemical potential of Li in the anode. Fig. 5 illustrates the calculated voltage of  $\text{Li}_x\text{Mn}_2\text{O}_4$  at 275 K. The voltage curve shows a large step of more than a volt at  $x=1$ . Since the lattice model applies only to cubic  $\text{Li}_x\text{Mn}_2\text{O}_4$ , this result clearly shows that the step is not a result of the coordinated Jahn–Teller distortion occurring around  $x=2$  [31]. Instead, it arises from the strong stability of stoichiometric  $\text{LiMn}_2\text{O}_4$ , where all the lithium ions reside in tetrahedral sites. The voltage step is a feature inherent to the spinel host structure and was also predicted for spinel  $\text{Li}_x\text{Co}_2\text{O}_4$ . The origin of the step was explored in detail in Ref. [27]. The plateau at 2 V between  $x=1$  and 2 is caused by the miscibility gap while the small step at  $x=1/2$  is the result of Li ordering.

#### 4. Effect of Jahn–Teller distortions

The results of the previous section show that many of the important properties of  $\text{Li}_x\text{Mn}_2\text{O}_4$  are qualitatively determined simply by a consideration of the interactions of the lithium ions with each other and with the host. The calculated voltage profile agrees qualitatively with experiment in that it exhibits a plateau between  $x=1$  and 2 [1,3,12], a step of more than a volt at  $x=1$  and a smaller step due to lithium ordering at  $x=1/2$  [9]. Furthermore, the results demonstrate that the two phase region between  $x=1$  and 2 can be predicted by neglecting the effect of

Jahn–Teller distortions. Despite the qualitative agreements, however, there are quantitative discrepancies, more so than is typical of first principles investigations of other lithium transition metal oxides [25,27,28,32–36]. Part of the quantitative discrepancy can be attributed to the neglect of Jahn–Teller distortions and related electronic phenomena.

In  $\text{Li}_x\text{Mn}_2\text{O}_4$ , Jahn–Teller distortions become more important with increasing lithium concentration as the number of Mn ions with effective valence of +3 increases. For this reason, the discrepancy is more severe at higher lithium concentration. Fig. 5 shows that the predicted voltage of the plateau between  $x=1$  and 2 is around 2 V which is almost a volt less than the experimental value. Part of the under-prediction results from the neglect of the cooperative Jahn–Teller distortion of  $\text{Li}_x\text{Mn}_2\text{O}_4$  around  $x=2$ . Since the tetragonally distorted form of  $\text{Li}_x\text{Mn}_2\text{O}_4$  is observed experimentally, it has a lower free energy than the cubic form. This is schematically illustrated in Fig. 6 where a hypothetical free energy curve for tetragonal  $\text{Li}_x\text{Mn}_2\text{O}_4$  is shown relative to the calculated free energy curve for cubic  $\text{Li}_x\text{Mn}_2\text{O}_4$ . From Eq. 3, it can be seen that the voltage is linearly related to the negative of the slope of the free energy curve of Fig. 6 (since the slope is equal to the chemical potential of Li). The correct free energy of tetragonal  $\text{Li}_x\text{Mn}_2\text{O}_4$  around  $x=2$  would, therefore, result in a decrease of the slope of the common tangent and hence an increase of the voltage plateau between  $x=1$  and 2. Although LDA

incorrectly predicts tetragonal  $\text{Li}_2\text{Mn}_2\text{O}_4$  to be energetically less stable than the cubic form [19], GGA finds the tetragonal form to be more stable and predicts an average voltage of 2.25 V between  $x=1$  and 2 when the effect of the cooperative Jahn–Teller distortion at  $x=2$  is included.

The predicted average voltage of 3.9 V between  $x=0$  and 1 is in reasonable agreement with the experimental value of 4.1 V, nevertheless, the predicted variation of the voltage profile in that concentration range is much larger than observed experimentally. As  $x$  approaches zero, the calculated voltage is 4.5 while at  $x=1$  it is 3.5. Experimentally, the voltage varies between 4.2 and 4.0. The discrepancy is likely a result of the inability of LDA to capture subtle electronic effects such as charge localization and local non-cooperative Jahn–Teller distortions. For example, in  $\text{LiMn}_2\text{O}_4$ , the average valence of Mn is 3.5. If the electrons are well localized, half the Mn ions would have a valence of +3 and the other half would have a valence of +4. The recent observation of charge ordering in  $\text{LiMn}_2\text{O}_4$  at low temperature demonstrates that this type of charge localization does occur in these compounds [5,6]. It is not unlikely that the charge localization persists at room temperature and for off-stoichiometric compositions even in the absence of long-range charge ordering. Furthermore, the oxygen octahedra around the  $\text{Mn}^{+3}$  ions are likely to undergo local Jahn–Teller distortions. Charge localization and accompanying local Jahn–Teller distortions, if present in actual crystals, even in the disordered state, should result in a lower energy as compared to that calculated with LDA which predicts delocalized electronic states. Furthermore, the distribution of  $\text{Mn}^{+3}$  and  $\text{Mn}^{+4}$  throughout the spinel crystal results in an additional configurational entropy. These energetic and entropic contributions become more important as  $x$  approaches 1 and hence will lower the free energy progressively more as the lithium concentration increases from  $x=0$ . The resulting reduction of the curvature of the free energy between  $x=0$  and 1 will produce a smaller variation in the voltage profile than was calculated by neglecting charge localization.

Throughout, we have omitted the orthorhombic form of  $\text{LiMn}_2\text{O}_4$  (which is stable below 280 K) from our phase diagram calculation [4,13–15]. Inclu-

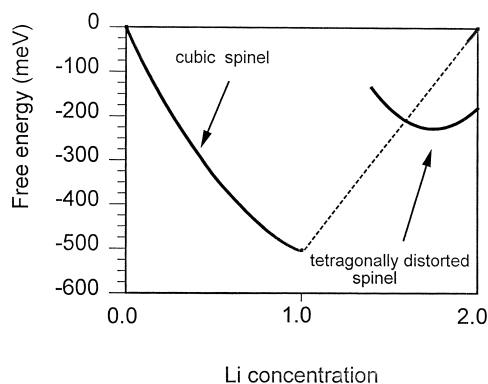


Fig. 6. Calculated free energy curve for cubic spinel  $\text{Li}_x\text{Mn}_2\text{O}_4$  as a function of Li concentration along with a hypothetical free energy curve of tetragonally distorted spinel in the vicinity of  $x=2$ . The free energy is per  $\text{Li}_{(x/2)}\text{MnO}_2$ .

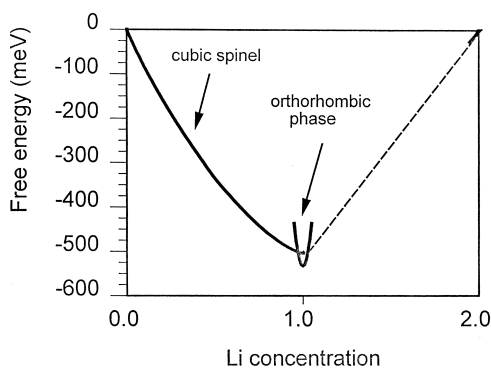


Fig. 7. Illustration of a hypothetical free energy curve for orthorhombic  $\text{Li}_x\text{Mn}_2\text{O}_4$  around  $x=1$  in relation to the calculated free energy curve for cubic spinel  $\text{Li}_x\text{Mn}_2\text{O}_4$  as a function of Li concentration. The free energy is per  $\text{Li}_{(x/2)}\text{MnO}_2$ .

sion of the orthorhombic phase will alter the topology of the calculated phase diagram slightly. To qualitatively ascertain the effect of the orthorhombic phase on the phase diagram, we can, as a first approximation, assign it a separate free energy curve as illustrated in Fig. 7. This is justified since the transition from cubic spinel to the orthorhombic form is observed to be first order [4]. Only below the transition temperature will the free energy of orthorhombic  $\text{Li}_x\text{Mn}_2\text{O}_4$  dip below that of cubic

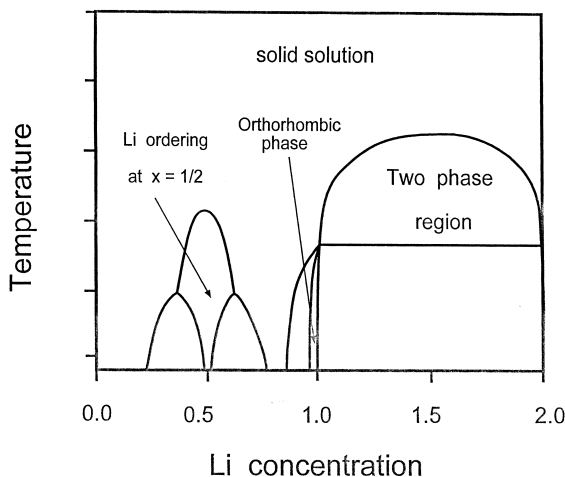


Fig. 8. Schematic illustration of how the orthorhombic phase may alter the calculated phase diagram of Fig. 2. Numerical values for the temperature scale have been omitted to emphasize that the phase diagram can only be viewed as a qualitative representation.

$\text{Li}_x\text{Mn}_2\text{O}_4$ . Since the orthorhombic form is produced by a complicated interplay between charge ordering and Jahn–Teller distortions [5,6]—the stability of which is very sensitive to the Mn valence—its free energy curve will likely be sharp as a function of lithium concentration. This is also supported by observations that the orthorhombic phase is stable in a very narrow concentration range around  $x=1$  [4,13]. Applying the common tangent construction to the free energy curves indicates that a two-phase region will separate cubic  $\text{Li}_x\text{Mn}_2\text{O}_4$  from orthorhombic  $\text{Li}_x\text{Mn}_2\text{O}_4$ . Qualitatively, therefore, we can expect the orthorhombic phase to affect the calculated phase diagram as illustrated in Fig. 8. In view of the uncertainties in the predicted transition temperatures in the calculated phase diagram of Fig. 2, we have omitted a numerical temperature scale.

## 5. Origin of volume change during first-order phase transformation

A major limitation of Mn-spinel cathodes is the capacity degradation that occurs when cycling over the 2.9 V plateau. The capacity loss is presumably associated with the large volume change (about 5.6%) and tetragonal distortion (about 16% increase in the  $c/a$  ratio) that accompany the cycling [1,3]. Although the tetragonal distortion is caused by the Jahn–Teller distortion, the origin of the large volume change is less clear. The volume change is in fact somewhat surprising since it does not occur in other spinel compounds. For example, experiments have shown that Li intercalation from  $x=1$  to 2 in  $\text{Li}_x\text{V}_2\text{O}_4$  [37] and  $\text{Li}_x\text{Ti}_2\text{O}_4$  [38] spinels change the volumes by 1.8% and  $-0.8\%$ , respectively. Similarly, our first-principles calculations show that Li intercalation from  $x=1$  to 2 in  $\text{Li}_x\text{Co}_2\text{O}_4$  and  $\text{Li}_x\text{Ni}_2\text{O}_4$  spinels change the volumes by 0.8% and 2.2%, respectively (it should be noted that spinel  $\text{LiNi}_2\text{O}_4$  is known to occur experimentally [39] while the stability of spinel  $\text{LiCo}_2\text{O}_4$  has been predicted from first-principles [22,35]). Understanding the origins of the volume effect in Mn-oxides may lead to suitably modified Mn-based materials with less volume expansion and consequently improved cyclability.

Three candidate sources for the large volume

expansion seen during intercalation from  $\text{LiMn}_2\text{O}_4$  to  $\text{Li}_2\text{Mn}_2\text{O}_4$  can be identified:

- (i) The introduction of more Li into the material and the shift of the Li from tetrahedral to octahedral sites ( $\Delta V_{\text{Li}}$ ).
- (ii) The Jahn–Teller distortion ( $\Delta V_{\text{JT}}$ ).
- (iii) The addition of electrons to the Mn anti-bonding  $e_g$  orbital ( $\Delta V_{e_g}$ ).

Each source of volume expansion has been assigned a symbol ( $\Delta V_{\text{XX}}$ ) which is given in parenthesis. Below we separate the contribution of each possible source of volume change.

To isolate the effect of Li addition and site movement we have performed first-principles non-spin-polarized calculations. In these calculations no magnetic moment is allowed, which means that the Mn  $e_g$  orbitals are not occupied and consequently the Jahn–Teller distortion is suppressed. The change in volume going from cubic  $\text{LiMn}_2\text{O}_4$  with Li in tetrahedral sites to cubic  $\text{Li}_2\text{Mn}_2\text{O}_4$  with Li in octahedral sites was found to be  $-1.3\%$ . This entire volume change is due to contribution (i) since the contributions of (ii) and (iii) have been excluded, so we set  $\Delta V_{\text{Li}} = -1.3\%$ . Notice that this small value is consistent with the results reported above for other spinels.

We can determine the effect of the Jahn–Teller distortion on volume by comparing the calculated volume of cubic  $\text{Li}_2\text{Mn}_2\text{O}_4$  spinel to the calculated volume corresponding to the Jahn–Teller distorted tetragonal  $\text{Li}_2\text{Mn}_2\text{O}_4$ . In this case we find that the volume expansion is  $2.2\%$ . Since all the  $\text{Mn}^{3+}$  ions undergo a Jahn–Teller distortion in this process we can estimate the effect of a Jahn–Teller distortion to be about  $2.2\%$  per Jahn–Teller ion.

The effect of the Jahn–Teller distortion on the volume in transforming from  $\text{LiMn}_2\text{O}_4$  to  $\text{Li}_2\text{Mn}_2\text{O}_4$  can now be estimated by the following argument. Recent evidence [4–6] indicates that even in  $\text{LiMn}_2\text{O}_2$  the octahedra around the  $\text{Mn}^{3+}$  ions are Jahn–Teller distorted. It is not unlikely that above room temperature this Jahn–Teller distortion is not cooperative. Hence, in going from  $\text{LiMn}_2\text{O}_4$  to  $\text{Li}_2\text{Mn}_2\text{O}_4$  a Jahn–Teller distortion is added to only half of the Mn ions, which should give a relative volume effect of about  $1.1\%$ . We therefore estimate

$\Delta V_{\text{JT}} = 1.1\%$ . This small value is consistent with our understanding of the Jahn–Teller distortion [40]. One expects the dominant effect of the electron-lattice coupling for a degenerate  $e_g$  electron to be a tetragonal deformation, so that little isotropic strain is produced.

We now turn to the final possible source for volume expansion, the increased occupation of the anti-bonding  $e_g$  orbital during Li intercalation. In  $\text{LiMn}_2\text{O}_4$  the average valence state of Mn is  $+3.5$ .  $\text{Mn}^{4+}$  has three electrons with parallel spin in  $t_{2g}$  states. Reduction of these  $\text{Mn}^{4+}$  upon lithiation of  $\text{LiMn}_2\text{O}_4$  adds an electron into an  $e_g$  level. While  $t_{2g}$  levels can be considered non-bonding,  $e_g$  states are anti-bonding combinations of metal d and oxygen p orbitals. Their filling should therefore be associated with a lengthening of the metal–oxygen bonds. Therefore, if we exclude the effect of the Jahn–Teller distortion, an isotropic lengthening of bonds is expected to occur during lithiation.

The volume effects of the  $e_g$  electrons can be calculated from first-principles in the following manner. Somewhat surprisingly, using first-principles methods it is possible to stabilize cubic  $\text{Li}_2\text{Mn}_2\text{O}_4$  in both a high-spin state (with each  $\text{Mn}^{3+}$  having four aligned electronic spins) and a semi-low-spin state (with each  $\text{Mn}^{3+}$  having two aligned and two anti-aligned electronic spins). The high-spin state, therefore, only differs from the low-spin state in that one  $t_{2g}$  electron is promoted to an  $e_g$  anti-bonding orbital in the former case. The increase in volume seen in going from the semi-low spin state to the high-spin state is hence approximately a measure of the change in volume due to occupation of the  $e_g$  orbital. The high-spin state is expanded by  $12\%$  over the semi-low spin state. We will take this value to approximate the volume expansion each Mn contributes when it gains an  $e_g$  electron. During lithiation from  $\text{LiMn}_2\text{O}_4$  to  $\text{Li}_2\text{Mn}_2\text{O}_4$  an  $e_g$  electron is added to half of the Mn ions, enabling us to estimate  $\Delta V_{e_g} = 0.5 \times 12\% = 6.0\%$ .

We can now use the above results to write an equation for the total calculated volume expansion going from  $x=1$  to  $x=2$  in  $\text{Li}_x\text{Mn}_2\text{O}_4$

$$\begin{aligned} \Delta V_{\text{tot}} &= \Delta V_{\text{Li}} + \Delta V_{\text{JT}} + \Delta V_{e_g} \\ &= -1.3\% + 1.1\% + 6.0\% = 5.8\%, \end{aligned}$$

which is quite close to the value of 5.6% measured experimentally [3].

These results give interesting insights as to the cause of the volume strain when  $\text{LiMn}_2\text{O}_4$  is further lithiated. While the Jahn–Teller distortion does lead to a positive volume contribution, by far the biggest effect comes from the anti-bonding  $e_g$  electron that is added when  $\text{Mn}^{4+}$  is reduced to  $\text{Mn}^{3+}$ . This leads to interesting possibilities for suppressing the volume increase in lithiated-manganese oxides. The volume expansion could be significantly decreased if it were possible to suppress the promotion of the electron from the Li into the anti-bonding  $e_g$  orbital. While  $\text{Mn}^{3+}$  obviously always needs four valence electrons, it may be possible to influence the competition between the crystal field splitting and the intra-ionic exchange which determines the sequence of level filling (see Fig. 9). It is well known that the crystal field and the covalent interactions with the ligands splits the five d orbitals on Mn into a lower three-fold degenerate  $t_{2g}$  band and an upper two-fold degenerate  $e_g$  band. The intra-ionic exchange interaction (which is responsible for Hund's rules) adds a significant energy penalty for filling identical levels with anti-parallel spins. This is schematically represented in Fig. 9 by showing separate levels for the up and down spin of the electron (up and down can obviously be assigned arbitrarily). Although the separation between  $t_{2g}$  and  $e_g$  levels of the same spin is caused by the crystal field, the separation between

identical levels of opposite spin is caused by the exchange interaction. In  $\text{Mn}^{3+}$  the lowest down-spin  $t_{2g}$  level is usually still above the first up-spin  $e_g$  level, resulting in a fully high-spin  $\text{Mn}^{3+}$  ion.

While it is not clear how to modify the intra-ionic exchange, the crystal field splitting depends on the Mn–O bond length. Compressing this bond would lead to an increase in the splitting to the point where the up-spin  $e_g$  level rises above the lowest down-spin  $t_{2g}$  level. At this point we would obtain a semi-low spin  $\text{Mn}^{3+}$  with a net two-electron spin and no  $e_g$  electron. From our previously established understanding such a system would have a lower volume.

We investigated this effect in more detail using first-principles methods. Fig. 10 shows the energy versus volume for three different symmetries and spin configurations. For each curve, the minimum corresponds to the equilibrium energy and volume for a system with a given symmetry and electron configuration. Note that the Jahn–Teller distorted structure with high-spin  $\text{Mn}^{3+}$  has the overall lowest energy, in agreement with experiments [1,3]. Clearly the  $e_g$  electron is the key quantity which causes the volume expansion, not the Jahn–Teller distortion. We have also performed similar calculations for  $\text{LiMnO}_2$  in the layered  $\alpha\text{-NaFeO}_2$  structure and found the same trend as with the spinel. The layered structure also shows a small change in volume associated with the Jahn–Teller distortion and a larger change in volume associated with the occupation of the  $e_g$  orbital.

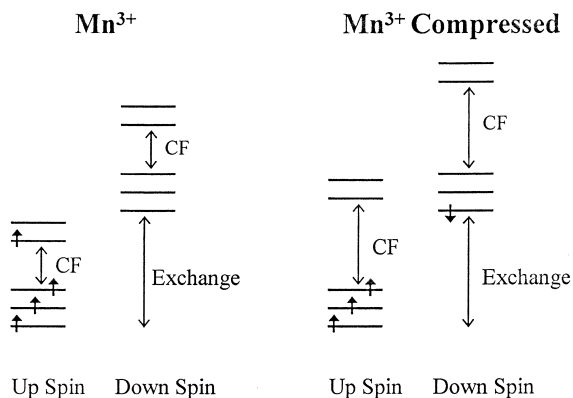


Fig. 9. Schematic illustration of the effect of compression of the Mn–O bond lengths on the magnetic moment on the Mn ion. Level splittings induced by the crystal structure are labeled CF.

## 6. Conclusions

We have investigated important phase transformations and their accompanying volume changes in  $\text{Li}_x\text{Mn}_2\text{O}_4$  from first principles. We have shown that a first-principles lattice model that describes the energetics of lithium ions and vacancies distributed over the 8a and 16c sites of the spinel  $\text{Mn}_2\text{O}_4$  host structure predicts Li ordering at  $x=1/2$  and a miscibility gap between  $x=1$  and 2. Furthermore, the voltage curve predicted by the lattice model at non-zero temperature exhibits a step of around a volt at  $x=1$ , a prominent feature of the experimental voltage curve of spinel  $\text{Li}_x\text{Mn}_2\text{O}_4$ . Since the lattice model neglects the effects of Jahn–Teller distortions

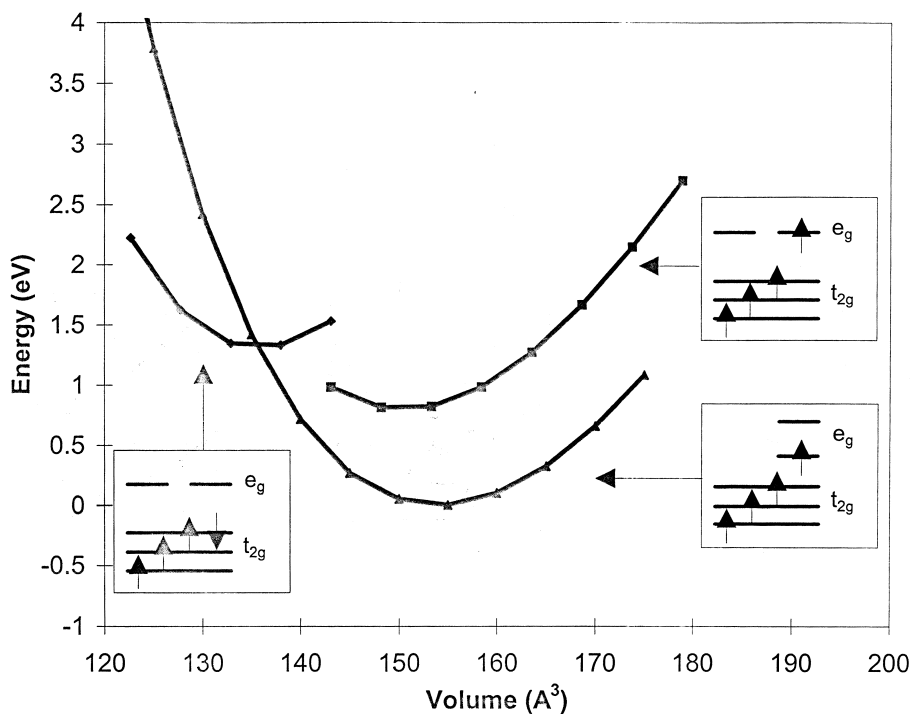


Fig. 10. The energy versus volume for cubic spinel  $\text{Li}_2\text{Mn}_2\text{O}_4$  with low spin Mn, cubic spinel  $\text{Li}_2\text{Mn}_2\text{O}_4$  with high spin Mn and tetragonally distorted (due to the Jahn–Teller distortion) spinel  $\text{Li}_2\text{Mn}_2\text{O}_4$  with high spin Mn. Energy and volume are for a spinel primitive unit cell (i.e.  $\text{Li}_4\text{Mn}_4\text{O}_8$ ).

and related localized electronic phenomena, these results demonstrate that the voltage step at  $x=1$  and the two-phase region are not driven by Jahn–Teller distortions. We have also indicated how Jahn–Teller distortions can affect the phase diagram and the voltage curve. Finally, our first-principles total energy calculations indicate that the major contribution to the volume change associated with the first order transition between  $x=1$  and 2 is the transfer of the electrons of Li to the Mn anti-bonding  $e_g$  orbital.

### Acknowledgements

This work was supported by the Department of Energy, Office of Basic Energy Sciences under Contract No. DE-FG02-96ER45571 and by the MRSEC Program of the National Science Foundation under award number DMR 98-08941. Computing was supported by NSF cooperative agreement

ACI-9619020 through computing resources provided by the National Partnership for Advanced Computational Infrastructure (NPACI) at the San Diego Supercomputing Center. AVDV gratefully acknowledges support from the DOE Computational Science Graduate Fellowship Program.

### References

- [1] M.M. Thackeray, W.I.F. David, P.G. Bruce, J.B. Goodenough, *Mat. Res. Bull.* 18 (1983) 461–472.
- [2] M.M. Thackeray, P.J. Johnson, L.A. de Picciotto, P.G. Bruce, J.B. Goodenough, *Mat. Res. Bull.* 19 (1984) 179.
- [3] T. Ohzuku, M. Kitagawa, T. Hirai, *J. Electrochem. Soc.* 137 (1990) 769–775.
- [4] A. Yamada, M. Tanaka, *Mater. Res. Bull.* 30 (1995) 715.
- [5] J. Rodríguez-Carvajal, G. Rouse, C. Masquelier, M. Hervey, *Phys. Rev. Lett.* 81 (1998) 4660–4663.
- [6] G. Rouse, C. Masquelier, J. Rodríguez-Carvajal, M. Hervey, *Electrochem. Solid-State Lett.* 2 (1999) 1–3.

- [7] J.E. Greedan, N.P. Raju, A.S. Will, C. Morin, S.M. Shaw, J.N. Reimers, *Chem. Mater.* 10 (1998) 3058–3067.
- [8] M.M. Thackeray, *Prog. Solid. State Chem.* 25 (1997) 1–71.
- [9] J.B. Goodenough, M.M. Thackeray, W.I.F. David, P.G. Bruce, *Revue de Chimie Minerale* 21 (1984) 435–455.
- [10] W. Liu, K. Kowal, G.C. Farrington, *J. Electrochem. Soc.* 145 (1998) 459–465.
- [11] X.Q. Yang, X. Sun, S.J. Lee, J. McBreen, S. Mukerjee, M.L. Daroux, X.K. Xing, *Electrochem. Solid-State Lett.* 2 (1999) 157.
- [12] J.M. Tarascon, E. Wang, F.K. Shokoohi, W.R. McKinnon, S. Colson, *J. Electrochem. Soc.* 138 (1991) 2859–2864.
- [13] A. Yamada, *J. Solid State Chem.* 122 (1996) 160.
- [14] J. Tabuchi, T. Numata, Y. Shimakawa, M. Shirakata, *Mater. Res. Soc. Symp. Proc.* 496 (1998) 287.
- [15] H. Hayakawa, T. Takada, H. Enoki, E. Akiba, *J. Mater. Sci. Lett.* 17 (1998) 811.
- [16] H. Abiko, M. Hibino, T. Kudo, *Electrochem. Solid State Lett.* 1 (1998) 114–116.
- [17] P. Hohenberg, W. Kohn, *Phys. Rev.* 136 (1964) 864.
- [18] W. Kohn, L.J. Sham, *Phys. Rev.* A140 (1965) 1133.
- [19] S.K. Mishra, G. Ceder, *Phys. Rev.* B59 (1999) 6120–6130.
- [20] G. Kresse, J. Furthmüller, *Comput. Mat. Sci.* 6 (1996) 15–50.
- [21] G. Kresse, J. Furthmüller, *Phys. Rev.* B54 (1996) 11169.
- [22] G. Ceder, A. Van der Ven, *Electrochimica Acta* 45 (1999) 131–150.
- [23] D. de Fontaine, in: H. Ehrenreich, D. Turnbull (Eds.), *Solid State Physics*, Vol. 47, Academic Press, 1994, pp. 33–176.
- [24] W.R. McKinnon, R.R. Haering, in: R.E. White, J.O.M. Backris, B.E. Conway (Eds.), *Modern Aspects of Electrochemistry*, Vol. 15, Plenum, New York, 1983, p. 235.
- [25] A. Van der Ven, M.K. Aydinol, G. Ceder, *J. Electrochem. Soc.* 145 (1998) 2149–2155.
- [26] A. Van der Ven, M.K. Aydinol, G. Ceder, G. Kresse, J. Hafner, *Phys. Rev.* B58 (1998) 2975–2987.
- [27] A. Van der Ven, G. Ceder, *Phys. Rev.* B59 (1999) 742–749.
- [28] C. Wolverton, A. Zunger, *J. Power Sources* 82 (1999) 680–684.
- [29] J.M. Sanchez, F. Ducastelle, D. Gratias, *Physica* 128A (1984) 334–350.
- [30] G.D. Garbulsky, G. Ceder, *Phys. Rev.* B51 (1995) 67–72.
- [31] M.K. Aydinol, G. Ceder, *J. Electrochem. Soc.* 144 (1997) 3832–3835.
- [32] M.K. Aydinol, A.F. Kohan, G. Ceder, K. Cho, J. Joannopoulos, *Phys. Rev.* B56 (1997) 1354–1365.
- [33] E. Deiss, A. Wokaun, J.-L. Barras, C. Daul, P. Dufek, *J. Electrochem. Soc.* 144 (1997) 3877–3881.
- [34] L. Benco, J.L. Barras, M. Atanasov, C.A. Daul, E. Deiss, *Solid State Ionics* 112 (1998) 225–259.
- [35] C. Wolverton, A. Zunger, *J. Electrochem Soc.* 145 (1998) 2424–2431.
- [36] R. Benedek, M.M. Thackeray, L.H. Yang, *Phys. Rev.* B60 (1999) 6335–6342.
- [37] G. Pistoia, M. Pasquali, L.A. de Picciotto, M.M. Thackeray, *Solid State Ionics* 28 (1988) 879.
- [38] R.J. Cava, D.W. Murphy, S. Zahurak, A. Santoro, R.S. Roth, *J. Solid State Chem.* 53 (1984) 64–75.
- [39] M.G.S.R. Thomas, W.I.F. David, J.B. Goodenough, P. Groves, *Mat. Res. Bull.* 20 (1985) 1137–1146.
- [40] K. Kugel, D.I. Khomskil, *Sov. Phys. Usp.* 25 (1982) 231–256.